THE JOURNAL OF PHYSICAL CHEMISTRY Letters

Letter

pubs.acs.org/JPCL

Theoretical Understanding of Mechanisms of Proton Exchange Membranes Made of 2D Crystals with Ultrahigh Selectivity

Le Shi,[†] Ao Xu,[†] Guanhua Chen,[‡] and Tianshou Zhao*[,†]

[†]Department of Mechanical and Aerospace Engineering, The Hong Kong University of Science and Technology, Clear Water Bay, Kowloon, Hong Kong, China

[‡]Department of Chemistry, The University of Hong Kong, Pokfluam Road, Hong Kong, China

Supporting Information

ABSTRACT: Recent reports on proton conduction across pristine graphene and hexagonal boron nitride (h-BN) provide a new avenue for the design of proton exchange membranes. The uniform pores formed by the electron clouds of two-dimensional (2D) crystals can effectively block the undesired transportation of other species thus ultrahigh selectivity can be achieved. With the aid of first-principles calculations, we investigate the proton conduction process across six kinds of intact 2D crystals, namely graphene, h-BN, β_{12} boron sheet, χ_3 boron sheet, phosphorene, and silicene. To clarify the proton conduction mechanism, three proton penetration modes are proposed: dissociation-penetration, adsorption-penetration, and direct penetration. Based on our calculation results, for graphene and h-BN without atomic defects, they are unlikely to provide sufficient proton conductivity at room temperature when no bias potential is applied. By contrast, the β_{12} boron sheet, χ_3 boron sheets, and silicene exhibit relatively lower proton penetration energy barriers, making them prospective candidates for future proton exchange membrane applications.

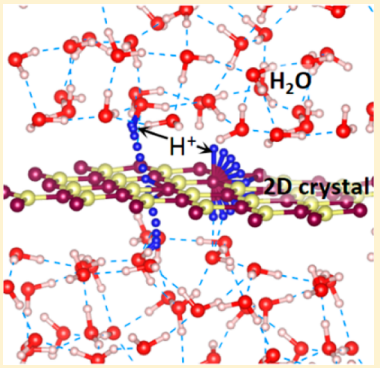

Due to their atomically thin structure, two-dimensional (2D) materials have emerged as a new family of building blocks for membranes which are expected to achieve low transport resistance as well as high selectivity.[1−5] Most of previous works concentrated on creating pores on 2D materials to achieve desired selectivity for gas[6−9] or ion separation.[10−14] Significant progress have also been achieved on employing the graphene oxide nanosheets to serve as the selective proton exchange membranes.[15−17] Recently, Geim's group reported that the pristine 2D crystals, graphene, and hexagonal boron nitride (h-BN), can conduct protons via the uniform pores formed by the in-plane electron clouds with low energy barriers (0.78 eV for graphene and 0.30 eV for h-BN), thus can be used as proton exchange membrane in fuel cells[18] and isotope separation devices.[19] Follow-up experiments by our group[20] and Holmes et al.[21] also demonstrated that when sandwiching a chemical vapor deposition (CVD) grown graphene or h-BN layer in Nafion membrane, the methanol crossover issue in direct methanol fuel cells (DMFCs) can be significantly suppressed.

However, how protons conduct across 2D crystals in aqueous environment is still unclear, and whether intact graphene or h-BN can provide sufficient proton conductivity is under debate. Some researchers argue that the observed proton conductivity mainly come from the rare atomic defects.[22,23] First-principles calculations have shown that, in a vacuum environment, if the protons penetrate graphene or h-BN via a metastable physisorption state, the energy barriers are about 1.25−1.56 eV for graphene and 0.70−0.91 eV for h-BN,[18,24−26] a bit higher than those deduced from experiments. Considering other factors such as the quantum nuclear effects (QNEs), bias potential and hydrogen adsorption, the proton penetration energy barriers can be further lowered, which may explain the experimental observations. However, if considering the much more stable chemisorption state of proton, the calculated energy barriers would be much higher (>3.0 eV).[26] Moreover, the experiments were conducted in aqueous environment where the protons mainly exist in the form of hydronium ions (H_3O^+) instead of bare protons (H^+), thus the vacuum environment assumption in previous calculations is oversimplified. Calculations incorporating explicit water molecules shown that the proton penetration in aqueous environment across intact graphene or h-BN is nearly impossible at room temperature with energy barriers higher than 3.0 eV, where a proton is assumed to first dissociate from a hydronium ion and then penetrate the 2D crystals and combine with another water molecule to form a new hydronium ion.[23,26] Other possible proton penetration modes or other 2D crystals that exhibit lower proton penetration energy barriers are still yet to be explored.

In this Letter, we investigate the proton conduction process across six kinds of 2D crystals, namely graphene, h-BN, β_{12} boron sheet,[27] χ_3 boron sheet,[27] phosphorene[28] and silicene.[29] To clarify the proton conduction mechanism, three proton

Received: August 1, 2017
Accepted: August 28, 2017
Published: August 28, 2017

DOI: 10.1021/acs.jpclett.7b01999
J. Phys. Chem. Lett. 2017, 8, 4354−4361

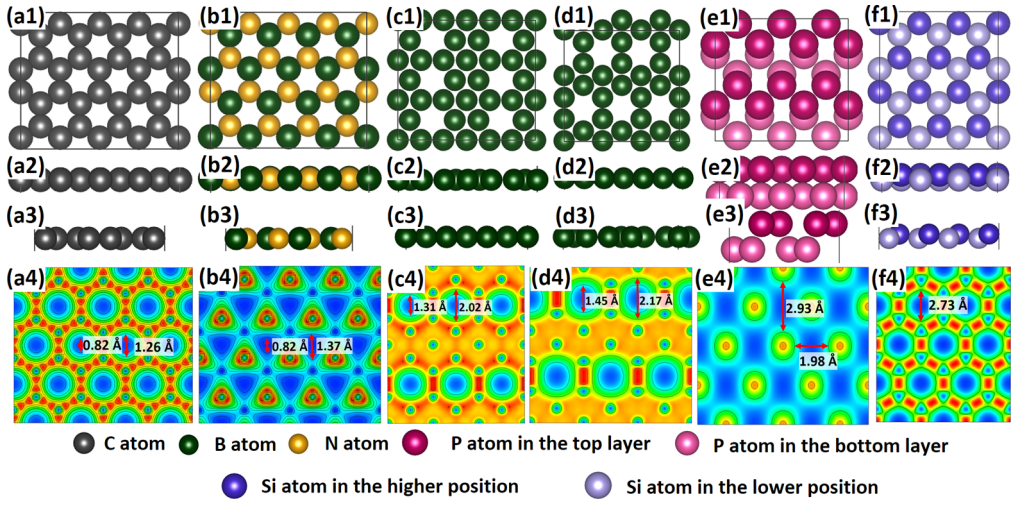

Figure 1. Geometries and charge density plots of (a) graphene, (b) h-BN, (c) β_{12} boron sheet, (d) χ_3 boron sheet, (e) phosphorene, and (f) silicene. The contour line in the charge density plots represents 0.05 e/Bohr^3.

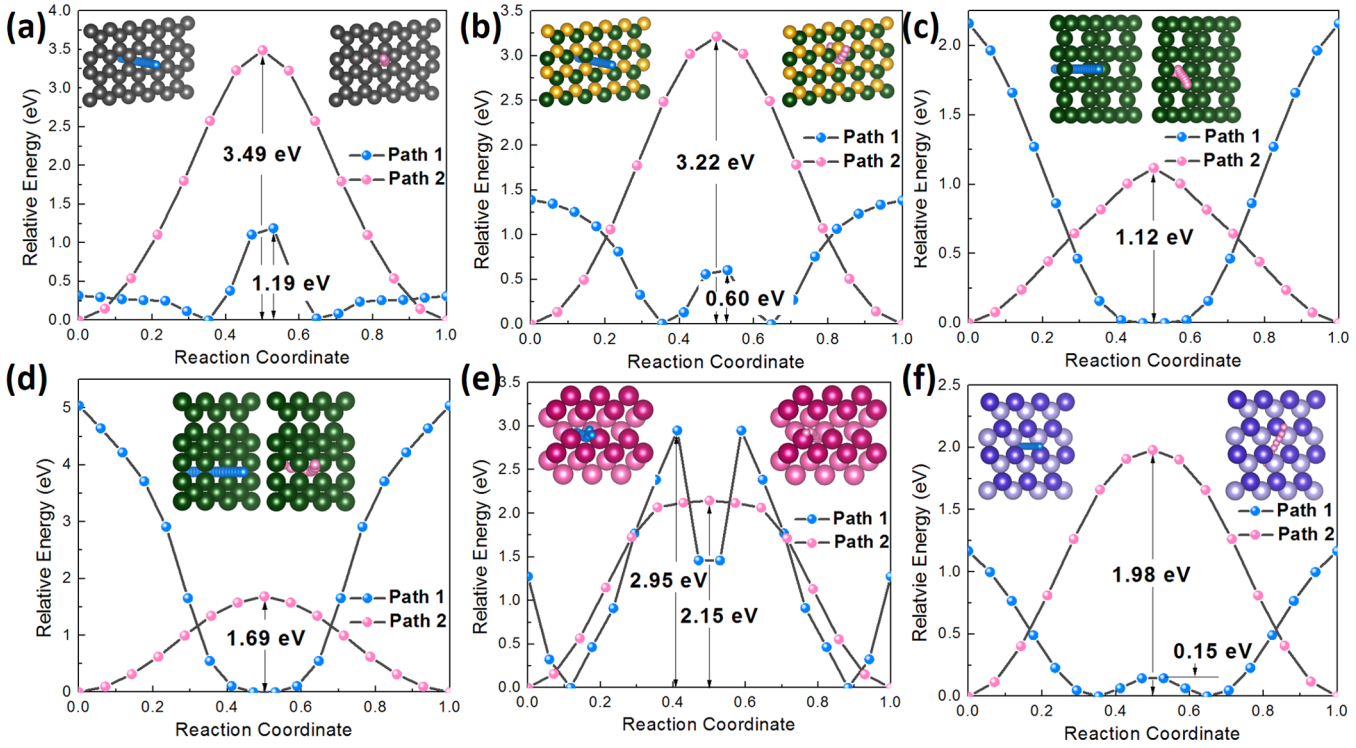

Figure 2. Proton conduction across (a) graphene, (b) h-BN, (c) β_{12} boron sheet, (d) χ_3 boron sheet, (e) phosphorene, and (f) silicene in a vacuum environment.

penetration modes: dissociation-penetration, adsorption-penetration, and direct penetration are proposed. The proton penetration energy barriers across the 2D crystals in aqueous environment incorporating explicit water molecules are calculated using the density functional theory (DFT) method. Our work shed light on the proton conduction mechanism across 2D crystals and identified promising candidates for future proton exchange membrane application.

DFT calculations were performed using the ABINIT[30−32] software package. Perdew−Burke−Ernzerhof (PEB) general gradient approximation (GGA)[33] and projector augmented wave (PAW)[34] pseudopotentials were employed to treat the exchange-correlation functionals and electron−ion interactions. Grimme's D2 correction[35] was adopted to describe the van der Waals interaction. For geometrical optimization, all the atoms were fully relaxed to reach a force tolerance of 0.01 eV/Å^{-1}. Proton penetration energy barriers were calculated using the climbing image nudged elastic band (CI-NEB) method.[36] For calculations considering vacuum environment, a 15 Å vacuum gap was added to prevent the interaction between slabs. The cutoff energy was set to be 20 Ha and the k-point mesh was set to be 3 × 3 × 2. Constrained minima hopping algorithm[37] implemented in the Atomic Simulation Environment (ASE)[38] was used to determine the stable H_2O and H_3O^+ adsorption configurations on 2D crystals. For each 2D crystal adsorbed with H_2O or H_3O^+, 20 minima hopping steps were performed,

DOI: 10.1021/acs.jpclett.7b01999
J. Phys. Chem. Lett. 2017, 8, 4354−4361

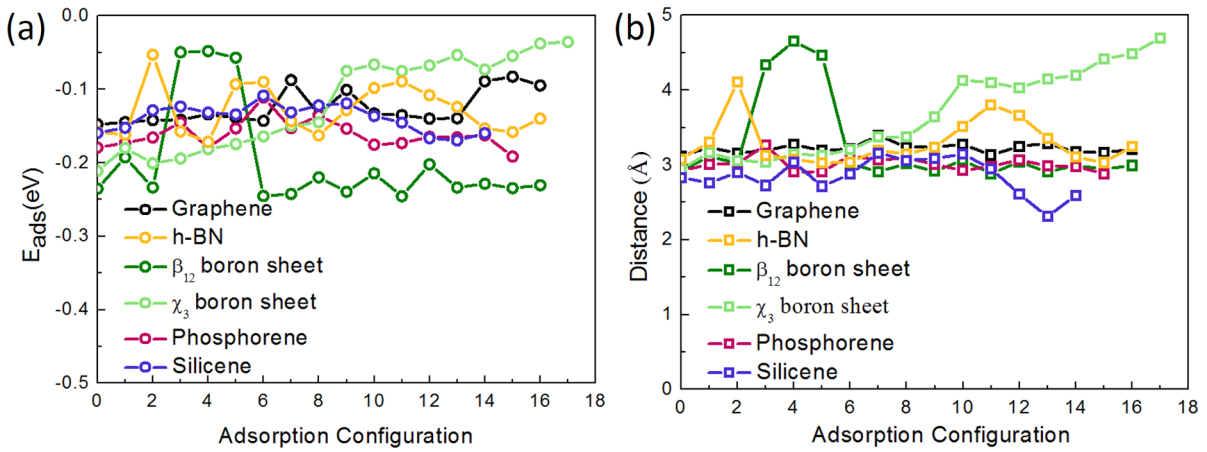

Figure 3. (a) H_2O adsorption energies and (b) the distances between H_2O and 2D crystals of the searched stable adsorption configurations.

and the corresponding geometries of the identified local minima were used to further calculate the adsorption energies. For a neutral system, the adsorption energy was calculated as

$$E_{ads} = E_{total} - E_{substrate} - E_{adsorbate} \quad (1)$$

where E_{total}, $E_{substrate}$, and $E_{adsorbate}$ represent the energy of the total system, the 2D crystal, and the adsorbate. For a charged system, the adsorption energy was calculated as[39]

$$E_{ads} = E_a - E_f \quad (2)$$

where E_a is the energy of the system with adsorbate adsorbed on 2D crystals, and E_f is the energy of the system putting adsorbate far away from 2D crystals.

To prepare the aqueous environment, water molecules were put evenly into the vacuum space to ensure that the density of water in the supercell is close to 1 g/cm^3, which is the experimental value under standard conditions. Then the system went through 50 minima hopping steps to search for the low-lying energy minima in the water configuration space.[40] The configuration with the lowest energy was then identified for further calculations. For calculations considering aqueous environment, the cutoff energy was set to be 15 Ha, and the k-point mesh was set to be $2 \times 2 \times 1$. It should be noted that in the calculations on proton conduction in aqueous environment, the calculated energy barriers depend on the water configurations, thus only a qualitative description for the proton conduction process can be provided. In our future work, calculations incorporating the dynamic nature of aqueous environment[23,41−44] will be conducted.

The optimized geometries and electron density distribution of considered 2D crystals are shown in Figure 1a−f. To compare the pore size formed by electron clouds, we plot the contour line of 0.05 e/Bohr^3 and define the area enclosed by the first contour line to be the pore size. Graphene and h-BN show the smallest pore size of 0.82 Å, while the β_{12} and χ_3 boron sheet show much larger pore size of 1.31 and 1.45 Å. Different from the other cases, the pores formed by the electron clouds of phosphorene and silicene are three-dimensional (3D), as shown in Figure S1. Phosphorene exhibits a puckered structure with a height of 2.12 Å, and silicene exhibits a slightly buckled structure with a height of 0.46 Å. Figure 1e4,f4 show the midplane cross-section of their charge density distribution. The narrowest sizes of the 3D pores are 1.98 Å for phosphorene and 2.74 Å for silicene.

We first calculated the proton penetration energy barriers across 2D crystals in vacuum environment as benchmark. Two penetration routes are considered: the one with both ends fixed 3 Å above the mid of the pores formed by the 2D crystals (path 1); and the one with both ends relaxed to the most stable proton adsorption sites on the 2D crystals (path 2). For path 1, the penetration energy profiles are plotted in blue spheres in Figure 2a−f. Graphene and h-BN exhibit energy barriers of 1.19 and 0.60 eV, respectively, which show good agreement with previous studies.[18,25] β_{12} and χ_3 boron sheets show zero proton penetration energy barrier, which are resulted from the electron deficiency of boron atoms. Phosphorene shows an energy barrier as high as 2.95 eV, and the proton penetration route is zigzag instead of straight, which is caused by the complex geometry of its electron density distribution, as shown in Figure S2. For silicene, as the pore size formed by the electron clouds is large and the bukeling is slight, proton can still maintain a direct penetration route and shows a low energy barrier of 0.15 eV. For path 2, Table S1 lists the proton adsorption energy on 2D crystals. All the 2D crystals show strong chemical adsorption toward proton. The proton penetration energy profiles following path 2 are plotted in pink spheres in Figure 2a−f. For most cases, the proton penetration energy barriers of path 2 are much higher than those of path 1. The only exception is phosphorene, where path 2 shows a smoother penetration route and lower penetration energy barrier.

To investigate whether these 2D crystals can effectively block the transportation of other species, we calculated the penetration energy barriers of H_3O^+ and CH_3OH across β_{12} boron sheet, χ_3 boron sheet and silicene. Since graphene and h-BN show much denser electron distribution and the geometry of phosphorene is too complex, they are unlikely to allow the penetration of H_3O^+/CH_3OH. For β_{12} and χ_3 boron sheets, the H_3O^+ and CH_3OH molecules tend to dissociate as shown in Figure S4−S5 and Figure S9−S10, which is a result of the size-rejection effect, and indicates that these molecules cannot penetrate the 2D boron sheets. For silicene, the energy barriers are 5.85 eV for H_3O^+ (Figure S6−7) and 9.33 eV for CH_3OH (Figure S11−12), indicating that the penetration of H_3O^+ and CH_3OH are highly impossible to occur at room temperature. As the interactions between H_3O^+/CH_3OH and the aqueous phase are mainly weak hydrogen bonds, the calculated penetration energy barriers are expected to change little when considering the explicit water molecules. Thus, for all the 2D

DOI: 10.1021/acs.jpclett.7b01999
J. Phys. Chem. Lett. 2017, 8, 4354−4361

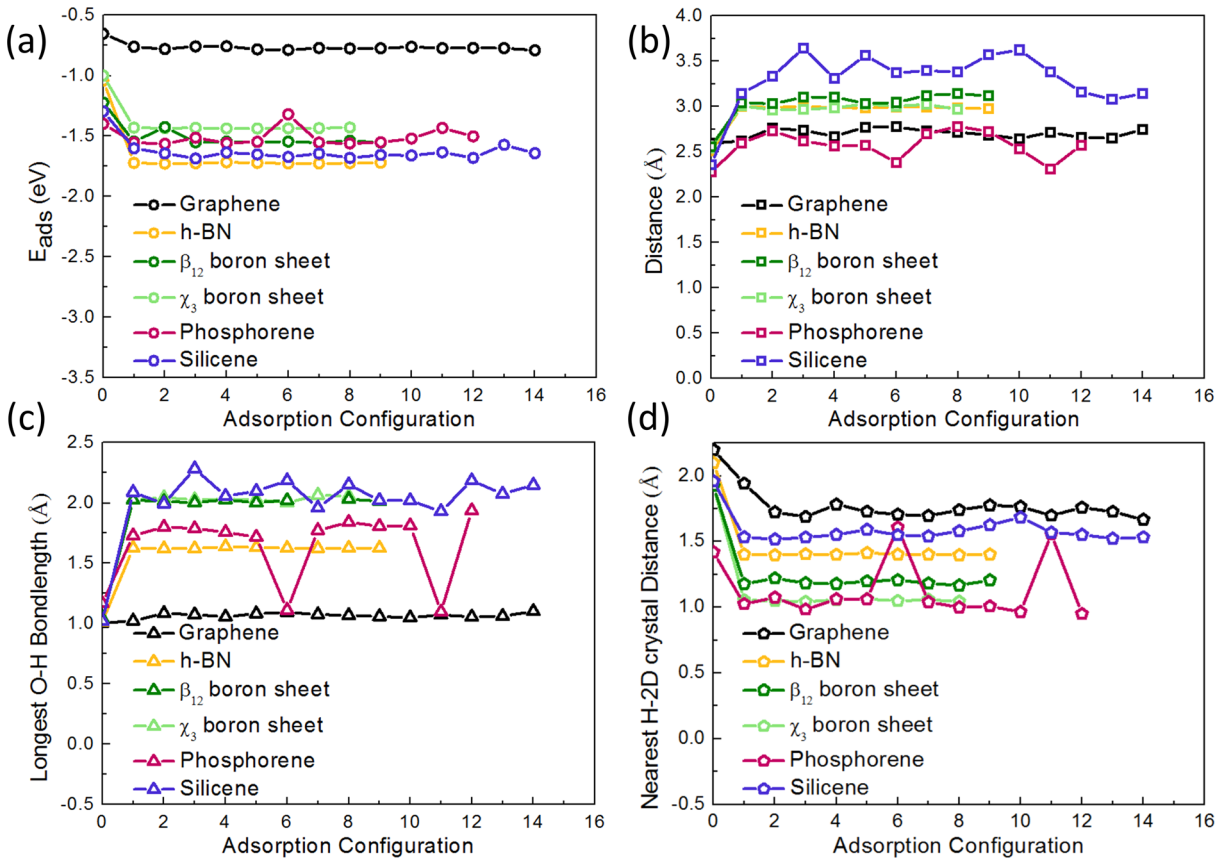

Figure 4. (a) H_3O^+ adsorption energies, (b) the distances between H_3O^+ and 2D crystals, (c) the longest O−H bondlengths of the adsorbed H_3O^+, and (d) the nearest H to 2D crystal distances of the searched adsorption configurations.

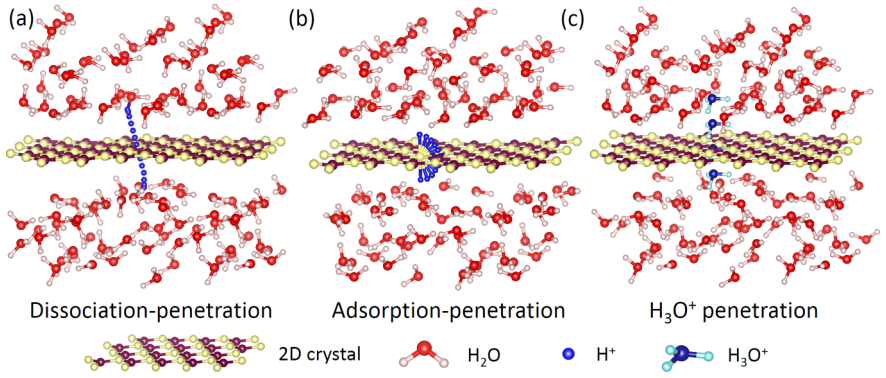

Figure 5. Proposed aqueous proton penetration modes.

crystals considered, effective blockage of H_3O^+/CH_3OH and larger species can be expected.

To study the detailed interactions between 2D crystals and the aqueous phase, we first investigated the adsorption behavior of a single H_2O/H_3O^+ molecule on 2D crystals. After 20 constrained minima hopping steps, stable adsorption configurations of H_2O and H_3O^+ on 2D crystals were identified. All the 2D crystals can maintain their atomic structures with a single H_2O adsorbed (Figure S14). The adsorption energies of H_2O with searched stable configurations on 2D crystals are plotted in Figure 3a, where the absolute value of all the adsorption energies are smaller than 0.25 eV. The distances between the mass center of H_2O molecule and 2D crystals are plotted in Figure 3b, where all the distances are larger than 2.3 Å. The calculation results show that the interactions between H_2O and 2D crystals are mainly weak van der Waals forces.

The adsorption energies of H_3O^+ with searched stable configurations on 2D crystals and the distances between H_3O^+ and 2D crystals are shown in Figure 4a,b, where all the 2D crystals show strong interactions with H_3O^+ except graphene. When analyzing the geometry of the adsorbed H_3O^+, the dissociation of H_3O^+ into a H_2O molecule and a proton adsorbed on the 2D crystals was observed for all the 2D crystals except graphene (Figure S15). The H_3O^+ dissociation can be reflected by the longest O−H bond length (>1.5 Å) (Figure 4c) and the nearest distance between the H atom and the 2D crystals (Figure 4d). For h-BN, β_{12} boron sheet, χ_3 boron sheet and silicene, the dissociation of H_3O^+ is strongly energetically preferred. By contrast, for phosphorene, the energy difference

DOI: 10.1021/acs.jpclett.7b01999
J. Phys. Chem. Lett. 2017, 8, 4354−4361

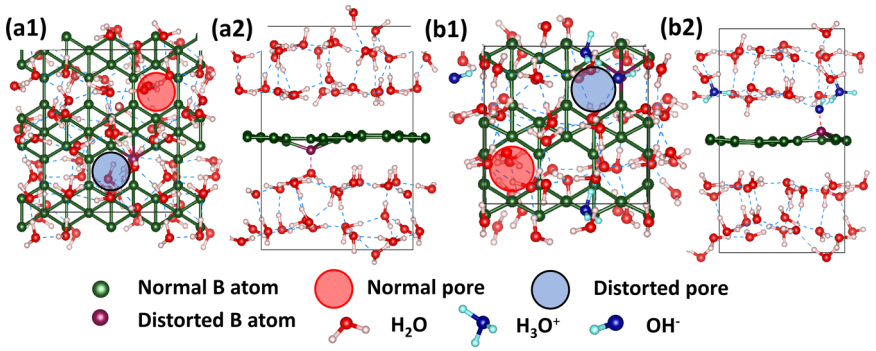

Figure 6. (a1,b1) Top and (a2,b2) side view of the distorted structure of β_{12} boron sheet and χ_3 boron sheet in an aqueous environment.

between the dissociated H_3O^+ adsorption configuration and intact H_3O^+ adsorption configuration is relatively small (<0.25 eV), thus both adsorption configurations appeared in the identified local minima. As H^+ shows much stronger adsorption toward the 2D crystals than H_2O as listed in Table S1, the H_3O^+ exhibits much larger adsorption energies than H_2O on the considered 2D crystals.

Based on the above findings that H_3O^+ prefers to dissociate into a H_2O molecule and a proton adsorbed on the surface for most 2D crystals considered, we propose three possible proton penetration modes. (i) Dissociation-penetration mode. As shown in Figure 5a, a proton first dissociate from a hydronium ion, penetrate across the 2D crystals and then combine with a water molecule to form another hydronium ion. (ii) Adsorption-penetration mode. As shown in Figure 5b, the proton may prefer to adsorb on the 2D crystals, and then flip over to the other side. (iii) Direct penetration mode. As shown in Figure 5c, this penetration mode involves the direct penetration of a hydronium ion and require large pore size of the 2D crystals. Since the pores of the considered 2D crystals can effectively block H_3O^+ transportation, the direct penetration mode will not be considered in the present work.

For all the prepared aqueous systems filled with explicit water molecules, a vacuum gap about 3.0 Å between the 2D crystals and the aqueous phase was observed (Table S3), which show good agreement with the weak interaction between 2D crystals and H_2O molecule calculated above. Due to the high flexibility of β_{12}/χ_3 boron sheets[45−47] and silicene,[29] structural distortion of the pores in these 2D crystals were observed. For the β_{12} boron sheet, a water molecule bonds with a boron atom as shown in Figure 6a, and the boron atom protrudes from the 2D plane, causing the distortion of neighboring pores. For the χ_3 boron sheet, a pair of water molecules self-dissociated into a hydronium ion and a hydroxide ion near the surface. The oxygen atom in the hydroxide ion forms a B−O bond with the protruded B atom as shown in Figure 6b, which also induced the distortion of the neighboring pores. Here we define the pores far away from the distorted B atom as "normal pore" and the pores contain the distorted B atom as "distorted pore". In the following, aqueous proton conduction across these two kinds of pores will be discussed separately. For silicene, water self-dissociation was also observed near the surface as shown in Figure S16. Several Si−O bonds with O come from both hydroxide ions and water molecules were formed. Since for silicene, all the pores are distorted to a certain degree in the supercell considered, we will only discuss the proton conduction through the distorted pores. The structural distortion phenomenon is not observed when calculating the adsorption energy of a single H_2O molecule on 2D crystals, which emphasizes the importance of incorporating explicit water molecules to study the proton conduction behavior in aqueous environment.

To study the aqueous proton conduction across 2D crystals following our proposed modes, the proton penetration energy barriers across the undistorted pores in graphene, h-BN, β_{12} and χ_3 boron sheets, and phosphorene were first calculated. An extra proton was introduced into the system either attached to a water molecule near the 2D crystals or adsorbed on the 2D crystals. The calculated energy barriers are listed in Table 1, and

Table 1. Proton Penetration Energy Barriers in Aqueous Phase Across the Undistorted Pores of 2D Crystals

	graphene	h-BN	β_{12} boron sheet (normal pore)	χ_3 boron sheet (normal pore)	phosphorene
$E_{b\_aq1}(\rightarrow)$/eV	4.31	3.55	1.82	1.97	2.55
$E_{b\_aq1}(\leftarrow)$/eV	5.05	3.68	1.38	0.91	2.44
$E_{b\_aq2}(\rightarrow)$/eV	3.34	3.03	1.16	1.21	1.89
$E_{b\_aq2}(\leftarrow)$/eV	3.39	3.32	0.96	1.10	2.01

the detailed energy profiles and geometries are provided in Figure S17−S36. We denote the dissociation-penetration mode and the adsorption-penetration mode as "aq1" and "aq2", respectively. The incorporation of aqueous environment introduces asymmetry in the energy profiles. We distinguish the two penetration energy barriers for a single case with " → " and " ← " to represent the reaction direction. For the dissociation-penetration mode, the energy barriers are >4.31 eV for graphene, > 3.55 eV for h-BN, and >2.44 eV for phosphorene. Thus, the dissociation-penetration mode is not feasible for these three 2D crystals at room temperature. By contrast, for the normal pores in the two kinds the boron sheets, the energy barriers can be as low as 1.38 and 0.91 eV. These values can be further lowered considering the possible influence of QNEs and bias potential, which makes possible the proton conduction across the normal pores of these two kinds of boron sheets at room temperature. For the adsorption-penetration mode, graphene, h-BN, and phosphorene also show high penetration energy barriers, which are hard to overcome at room temperature, while the β_{12} and χ_3 boron sheets exhibit much lower energy barriers close to 1.0 eV, making them promising choices for proton exchange membrane application.

Then we considered the proton penetration across the distorted pores in β_{12} boron sheet, χ_3 boron sheet, and silicene. For χ_3 boron sheet and silicene, as the self-dissociation of water

DOI: 10.1021/acs.jpclett.7b01999
J. Phys. Chem. Lett. 2017, 8, 4354−4361

molecules occur near the distorted pores, the conduction behavior of the proton in the self-dissociated H_3O^+ was also studied, and corresponding systems were labeled as the "neutral system". Accordingly, the systems containing the introduced extra proton were labeled as the "charged system". The calculated penetration energy barriers are listed in Table 2, and

Table 2. Proton Penetration Energy Barriers in Aqueous Phase Across the Distorted Pores in β_{12} Boron Sheet, χ_3 Boron Sheet, and Silicene

	β_{12} boron sheet (distorted pore)	χ_3 boron sheet (distorted pore)	silicene
$E_{b\_aq1}(\rightarrow)$/eV (neutral)	--	1.89	2.15
$E_{b\_aq1}(\leftarrow)$/eV (neutral)	--	1.29	1.58
$E_{b\_aq1}(\rightarrow)$/eV (charged)	1.30	1.96	1.62
$E_{b\_aq1}(\leftarrow)$/eV (charged)	1.69	1.53	1.15
$E_{b\_aq2}(\rightarrow)$/eV (charged)	0.25	0.55	2.04
$E_{b\_aq2}(\leftarrow)$/eV (charged)	0.063	1.32	1.39

the corresponding energy profiles and geometries can be found in Figure S37−S52. For the β_{12} boron sheet, the proton penetration energy barriers through the distorted pores following the dissociation-penetration mode are a bit lower than those through the normal pores, and the penetration energy barriers following the adsorption-penetration mode are much lower (0.063−0.25 eV) than those through the normal pores. For χ_3 boron sheet, the proton penetration energy barriers through the distorted pores following the dissociation-penetration mode are slightly higher than those through the normal pores for both neutral and charged systems. While for the adsorption-penetration mode, the energy barrier can be lowered to 0.55 eV, much lower than those calculated for the normal pores situation. For silicene, the proton penetration energy barriers through the distorted pores are >1.58 eV (neutral system) and >1.15 eV (charged system) following the dissociation-penetration mode, and >1.39 eV following the adsorption-penetration mode.

To qualitatively investigate which penetration mode is more likely to occur, we calculated the transformation energy barrier of a proton from the H_3O^+ mode to the adsorption mode. The initial state was constructed by randomly selecting a water molecule near the surface and attaching a proton to it. The final state was constructed by putting the attached proton to the nearest most stable adsorption sites of the 2D crystals. The energy barriers for the transformation process near the undistorted pores of graphene, h-BN, β_{12} and χ_3 boron sheets, and phosphorene are listed in Table 3, where ΔE represents the energy difference between the final and the initial state. The detailed energy profiles and geometries can be found in Figure S53−S62. For all the situations considered, ΔE are positive, indicating that the protons prefer to exist in the H_3O^+ form

Table 3. Transformation Energy Barriers for a Proton in H_3O^+ Mode to Adsorption Mode near the Undistorted Pores of 2D Crystals

	graphene	h-BN	β_{12} boron sheet (normal pore)	χ_3 boron sheet (normal pore)	phosphorene
$E_b(\rightarrow)$/eV	1.01	0.52	1.25	1.20	0.81
$E_b(\leftarrow)$/eV	0.06	0.24	0.65	0.83	0.60
ΔE/eV	0.95	0.28	0.60	0.37	0.21

instead of the adsorbed form near these 2D crystals, and the dissociation-penetration mode is more likely to occur for the proton conduction process. Compared with other cases, h-BN shows much lower transformation energy barriers along both two directions, indicating more frequent transformation between the two proton existing modes.

Then we calculated the transformation energy barriers for a proton in H_3O^+ mode to adsorption mode near the distorted atoms in β_{12}/χ_3 boron sheets and silicene as listed in Table 4.

Table 4. Transformation Energy Barriers for a Proton in H_3O^+ Mode to Adsorption Mode near the Distorted Atoms of β_{12}/χ_3 Boron Sheets and Silicene

	β_{12} boron sheet	χ_3 boron sheet	silicene
$E_b(\rightarrow)$/eV	1.23	1.75	0.046
$E_b(\leftarrow)$/eV	0.42	0.74	0.51
ΔE/eV	0.81	1.01	−0.46

The detailed energy profiles and geometries can be found in Figure S63−S68. For β_{12} and χ_3 boron sheet, the H_3O^+ mode is preferred for the proton over the adsorption mode near the distorted atoms, and the energy barriers for the transformation process are relatively high. By contrast, for silicene, protons in the adsorption mode show lower energy than protons in the H_3O^+ mode, and protons in the H_3O^+ mode can easily transform to the adsorption mode (E_b = 0.046 eV). Thus, for proton conduction across the distorted pores of β_{12} and χ_3 boron sheets, the dissociation-penetration mode is more likely to occur, while for the proton conduction across silicene, the adsorption-penetration mode is more likely to occur.

In conclusion, we studied the proton conduction behavior across six representative 2D crystals. To clarify the proton conduction mechanism, three penetration modes—dissociation-penetration, adsorption-penetration, and direct penetration—are proposed. Which penetration mode is more likely to occur depends on the detailed interactions among proton, aqueous phase, and 2D crystals. Based on the calculation results, proton penetration across graphene and h-BN are highly impossible at room temperature. The experimentally observed proton conductivity may be attributed to the atomic defects or bias potential. Although it possesses large electron pore size, the puckered structure of phosphorene strongly hinders the penetration of protons. The β_{12} boron sheet, χ_3 boron sheet, and silicene exhibit relatively lower proton penetration energy barriers, and can be expected to provide satisfied proton conductivity when serving as proton exchange membranes. Our study provides insight into the proton conduction mechanisms across 2D crystals in aqueous environment, and we identified the β_{12} boron sheet, χ_3 boron sheet, and silicene to be promising materials for proton exchange membrane application.

■ ASSOCIATED CONTENT

Supporting Information

The Supporting Information is available free of charge on the ACS Publications website at DOI: 10.1021/acs.jpclett.7b01999.

Charge density plots of 2D crystals; H^+ penetration route across phosphorene; H^+ adsorption energies and geometries on 2D crystals; geometries H_3O^+ and CH_3OH penetration across β_{12}/ χ_3 boron sheet and silicene; energy profiles and bond length changes of H_3O^+ and CH_3OH penetration across silicene; representative H_2O/

DOI: 10.1021/acs.jpclett.7b01999
J. Phys. Chem. Lett. 2017, 8, 4354−4361

H_3O^+ adsorption geometries on 2D crystals; density of water and the distances between aqueous phase and 2D crystals in the simulation box; geometries of silicene in aqueous environment; energy profiles and geometries of proton penetration across six kinds of 2D crystals following dissociation-penetration and adsorption-penetration modes; energy profiles and geometries for proton transformation from H_3O^+ form to adsorption form on the surfaces of 2D crystals. (PDF)

AUTHOR INFORMATION

Corresponding Author

*Tel.: (852) 2358 8647; E-mail: metzhao@ust.hk (T.S. Zhao).

ORCID

Le Shi: 0000-0003-1468-4549

Ao Xu: 0000-0003-0648-2701

Tianshou Zhao: 0000-0003-4825-2381

Notes

The authors declare no competing financial interest.

ACKNOWLEDGMENTS

The authors thank Professor Ding Pan (Department of Physics, HKUST) for his helpful discussion.The work described in this paper was supported by a grant from the Research Grants Council of the Hong Kong Special Administrative Region, China (Project No. HKUST9/CRF/11G).

REFERENCES

(1) Huang, L.; Zhang, M.; Li, C.; Shi, G. Graphene-Based Membranes for Molecular Separation. *J. Phys. Chem. Lett.* **2015**, *6*, 2806−2815.

(2) Zheng, Z.; Grünker, R.; Feng, X. Synthetic Two-Dimensional Materials: A New Paradigm of Membranes for Ultimate Separation. *Adv. Mater.* **2016**, *28*, 6529−6545.

(3) Liu, G.; Jin, W.; Xu, N. Two-Dimensional-Material Membranes: A New Family of High-Performance Separation Membranes. *Angew. Chem., Int. Ed.* **2016**, *55*, 13384−13397.

(4) Dervin, S.; Dionysiou, D. D.; Pillai, S. C. 2D Nanostructures for Water Purification: Graphene and Beyond. *Nanoscale* **2016**, *8*, 15115−15131.

(5) Wang, L.; Boutilier, M. S.; Kidambi, P. R.; Jang, D.; Hadjiconstantinou, N. G.; Karnik, R. Fundamental Transport Mechanisms, Fabrication and Potential Applications of Nanoporous Atomically Thin Membranes. *Nat. Nanotechnol.* **2017**, *12*, 509−522.

(6) Raghavan, B.; Gupta, T. H_2/CH_4 Gas Separation by Variation in Pore Geometry of Nanoporous Graphene. *J. Phys. Chem. C* **2017**, *121*, 1904−1909.

(7) Cranford, S. W.; Buehler, M. J. Selective Hydrogen Purification Through Graphdiyne Under Ambient Temperature and Pressure. *Nanoscale* **2012**, *4*, 4587−4593.

(8) Tao, Y.; Xue, Q.; Liu, Z.; Shan, M.; Ling, C.; Wu, T.; Li, X. Tunable Hydrogen Separation in Porous Graphene Membrane: First-Principle and Molecular Dynamic Simulation. *ACS Appl. Mater. Interfaces* **2014**, *6*, 8048−8058.

(9) Zhang, Y.; Shi, Q.; Liu, Y.; Wang, Y.; Meng, Z.; Xiao, C.; Deng, K.; Rao, D.; Lu, R. Hexagonal Boron Nitride with Designed Nanopores as a High-Efficiency Membrane for Separating Gaseous Hydrogen from Methane. *J. Phys. Chem. C* **2015**, *119*, 19826−19831.

(10) Walker, M. I.; Ubych, K.; Saraswat, V.; Chalklen, E. A.; Braeuninger-Weimer, P.; Caneva, S.; Weatherup, R. S.; Hofmann, S.; Keyser, U. F. Extrinsic Cation Selectivity of 2D Membranes. *ACS Nano* **2017**, *11*, 1340−1346.

(11) Sint, K.; Wang, B.; Král, P. Selective Ion Passage Through Functionalized Graphene Nanopores. *J. Am. Chem. Soc.* **2008**, *130*, 16448−16449.

(12) O'Hern, S. C.; Boutilier, M. S.; Idrobo, J. C.; Song, Y.; Kong, J.; Laoui, T.; Atieh, M.; Karnik, R. Selective Ionic Transport Through Tunable Subnanometer Pores in Single-Layer Graphene Membranes. *Nano Lett.* **2014**, *14*, 1234−1241.

(13) Celebi, K.; Buchheim, J.; Wyss, R. M.; Droudian, A.; Gasser, P.; Shorubalko, I.; Kye, J. I.; Lee, C.; Park, H. G. Ultimate Permeation Across Atomically Thin Porous Graphene. *Science* **2014**, *344*, 289−292.

(14) Heiranian, M.; Farimani, A. B.; Aluru, N. R. Water Desalination with a Single-Layer MoS_2 Nanopore. *Nat. Commun.* **2015**, *6*, 8616.

(15) Hatakeyama, K.; Karim, M. R.; Ogata, C.; Tateishi, H.; Funatsu, A.; Taniguchi, T.; Koinuma, M.; Hayami, S.; Matsumoto, Y. Proton Conductivities of Graphene Oxide Nanosheets: Single, Multilayer, and Modified Nanosheets. *Angew. Chem., Int. Ed.* **2014**, *53*, 6997−7000.

(16) Karim, M. R.; Hatakeyama, K.; Matsui, T.; Takehira, H.; Taniguchi, T.; Koinuma, M.; Matsumoto, Y.; Akutagawa, T.; Nakamura, T.; Noro, S. I.; et al. Graphene Oxide Nanosheet with High Proton Conductivity. *J. Am. Chem. Soc.* **2013**, *135*, 8097−8100.

(17) Tseng, C. Y.; Ye, Y. S.; Cheng, M. Y.; Kao, K. Y.; Shen, W. C.; Rick, J.; Chen, J. C.; Hwang, B. J. Sulfonated Polyimide Proton Exchange Membranes with Graphene Oxide Show Improved Proton Conductivity, Methanol Crossover Impedance, and Mechanical Properties. *Adv. Energy Mater.* **2011**, *1*, 1220−1224.

(18) Hu, S.; Lozada-Hidalgo, M.; Wang, F. C.; Mishchenko, A.; Schedin, F.; Nair, R. R.; Hill, E. W.; Boukhvalov, D. W.; Katsnelson, M. I.; Dryfe, R. A.; et al. Proton Transport Through One-Atom-Thick Crystals. *Nature* **2014**, *516*, 227−230.

(19) Lozada-Hidalgo, M.; Hu, S.; Marshall, O.; Mishchenko, A.; Grigorenko, A. N.; Dryfe, R. A.; Radha, B.; Grigorieva, I. V.; Geim, A. K. Sieving Hydrogen Isotopes Through Two-Dimensional Crystals. *Science* **2016**, *351*, 68−70.

(20) Yan, X. H.; Wu, R.; Xu, J. B.; Luo, Z.; Zhao, T. S. A Monolayer Graphene−Nafion Sandwich Membrane for Direct Methanol Fuel Cells. *J. Power Sources* **2016**, *311*, 188−194.

(21) Holmes, S. M.; Balakrishnan, P.; Kalangi, V.; Zhang, X.; Lozada-Hidalgo, M.; Ajayan, P. M.; Nair, R. R. 2D Crystals Significantly Enhance the Performance of a Working Fuel Cell. *Adv. Energy Mater.* **2017**, *7*, 1601216.

(22) Walker, M. I.; Braeuninger-Weimer, P.; Weatherup, R. S.; Hofmann, S.; Keyser, U. F. Measuring the Proton Selectivity of Graphene Membranes. *Appl. Phys. Lett.* **2015**, *107*, 213104.

(23) Achtyl, J. L.; Unocic, R. R.; Xu, L.; Cai, Y.; Raju, M.; Zhang, W.; Sacci, R. L.; Vlassiouk, I. V.; Fulvio, P. F.; Ganesh, P.; et al. Aqueous Proton Transfer Across Single-Layer Graphene. *Nat. Commun.* **2015**, *6*, 6539.

(24) Miao, M.; Nardelli, M. B.; Wang, Q.; Liu, Y. First Principles Study of the Permeability of Graphene to Hydrogen Atoms. *Phys. Chem. Chem. Phys.* **2013**, *15*, 16132−16137.

(25) Seel, M.; Pandey, R. Proton and Hydrogen Transport Through Two-Dimensional Monolayers. *2D Mater.* **2016**, *3*, 025004.

(26) Kroes, J. M.; Fasolino, A.; Katsnelson, M. I. Density Functional Based Simulations of Proton Permeation of Graphene and Hexagonal Boron Nitride. *Phys. Chem. Chem. Phys.* **2017**, *19*, 5813−5817.

(27) Feng, B.; Zhang, J.; Zhong, Q.; Li, W.; Li, S.; Li, H.; Cheng, P.; Meng, S.; Chen, L.; Wu, K. Experimental Realization of Two-Dimensional Boron Sheets. *Nat. Chem.* **2016**, *8*, 563−568.

(28) Kou, L.; Chen, C.; Smith, S. C. Phosphorene: Fabrication, Properties, and Applications. *J. Phys. Chem. Lett.* **2015**, *6*, 2794−2805.

(29) Houssa, M.; Dimoulas, A.; Molle, A. Silicene: A Review of Recent Experimental and Theoretical Investigations. *J. Phys.: Condens. Matter* **2015**, *27*, 253002.

(30) Gonze, X.; Beuken, J. M.; Caracas, R.; Detraux, F.; Fuchs, M.; Rignanese, G. M.; Sindic, L.; Verstraete, M.; Zerah, G.; Jollet, F.; et al. First-Principles Computation of Material Properties: the ABINIT Software Project. *Comput. Mater. Sci.* **2002**, *25*, 478−492.

(31) Gonze, X.; Amadon, B.; Anglade, P. M.; Beuken, J. M.; Bottin, F.; Boulanger, P.; Bruneval, F.; Caliste, D.; Caracas, R.; Côté, M.; et al. ABINIT: First-Principles Approach to Material and Nanosystem Properties. *Comput. Phys. Commun.* **2009**, *180*, 2582−2615.

DOI: 10.1021/acs.jpclett.7b01999
J. Phys. Chem. Lett. 2017, 8, 4354−4361

(32) Gonze, X. A Brief Introduction to the ABINIT Software Package. *Z. Kristallogr. - Cryst. Mater.* **2005**, *220*, 558−562.
(33) Perdew, J. P.; Ernzerhof, M.; Burke, K. Rationale for Mixing Exact Exchange with Density Functional Approximations. *J. Chem. Phys.* **1996**, *105*, 9982−9985.
(34) Blöchl, P. E. Projector Augmented-Wave Method. *Phys. Rev. B: Condens. Matter Mater. Phys.* **1994**, *50*, 17953.
(35) Grimme, S. Semiempirical GGA-Type Density Functional Constructed with a Long-Range Dispersion Correction. *J. Comput. Chem.* **2006**, *27*, 1787−1799.
(36) Henkelman, G.; Uberuaga, B. P.; Jónsson, H. A Climbing Image Nudged Elastic Band Method for Finding Saddle Points and Minimum Energy Paths. *J. Chem. Phys.* **2000**, *113*, 9901−9904.
(37) Peterson, A. A. Global Optimization of Adsorbate−Surface Structures While Preserving Molecular Identity. *Top. Catal.* **2014**, *57*, 40−53.
(38) Bahn, S. R.; Jacobsen, K. W. An Object-Oriented Scripting Interface to a Legacy Electronic Structure Code. *Comput. Sci. Eng.* **2002**, *4*, 56−66.
(39) Grosjean, B.; Pean, C.; Siria, A.; Bocquet, L.; Vuilleumier, R.; Bocquet, M. L. Chemisorption of Hydroxide on 2D Materials from DFT Calculations: Graphene versus Hexagonal Boron Nitride. *J. Phys. Chem. Lett.* **2016**, *7*, 4695−4700.
(40) Montemore, M. M.; Andreussi, O.; Medlin, J. W. Hydrocarbon Adsorption in an Aqueous Environment: A Computational Study of Alkyls on Cu (111). *J. Chem. Phys.* **2016**, *145*, 074702.
(41) Pan, D.; Galli, G. The Fate of Carbon Dioxide in Water-Rich Fluids Under Extreme Conditions. *Sci. Adv.* **2016**, *2*, e1601278.
(42) Pan, D.; Wan, Q.; Galli, G. The Refractive Index and Electronic Gap of Water and Ice Increase with Increasing Pressure. *Nat. Commun.* **2014**, *5*, 3919.
(43) Wolke, C. T.; Fournier, J. A.; Dzugan, L. C.; Fagiani, M. R.; Odbadrakh, T. T.; Knorke, H.; Jordan, K. D.; McCoy, A. B.; Asmis, K. R.; Johnson, M. A. Spectroscopic Snapshots of the Proton-Transfer Mechanism in Water. *Science* **2016**, *354*, 1131−1135.
(44) Hassanali, A.; Giberti, F.; Cuny, J.; Kühne, T. D.; Parrinello, M. Proton Transfer Through the Water Gossamer. *Proc. Natl. Acad. Sci. U. S. A.* **2013**, *110*, 13723−13728.
(45) Zhang, Z.; Yang, Y.; Penev, E. S.; Yakobson, B. I. Elasticity, Flexibility, and Ideal Strength of Borophenes. *Adv. Funct. Mater.* **2017**, *27*, 1605059.
(46) Karmodak, N.; Jemmis, E. D. The Role of Holes in Borophenes: An Ab Initio Study of Their Structure and Stability with and without Metal Templates. *Angew. Chem., Int. Ed.* **2017**, *56*, 10093.
(47) Sun, X.; Liu, X.; Yin, J.; Yu, J.; Li, Y.; Hang, Y.; Zhou, X.; Yu, M.; Li, J.; Tai, G.; Guo, W. Two-Dimensional Boron Crystals: Structural Stability, Tunable Properties, Fabrications and Applications. *Adv. Funct. Mater.* **2017**, *27*, 1603300.

DOI: 10.1021/acs.jpclett.7b01999
J. Phys. Chem. Lett. 2017, 8, 4354−4361